IRRADIATION EMBRITTLEMENT OF CLADDING AND HAZ OF RPV STEEL

J.S. LEE*, I.S. KIM[1], C.H. JANG[1] and A. KIMURA[2]
Korea Institute of S&T Evaluation and Planning
Dongwon Industry Bldg., 275, Yangjae-dong Seocho-gu, Seoul 137-130, Korea
[1]Korea Advanced Institute of Science and Technology
[2]Kyoto University, Gokasho, Uji, Kyoto 611-0011, Japan
*Corresponding author. E-mail : jslee@kistep.re.kr

Received July 25, 2005

Microstructural features and their related mechanical property changes in the 309L cladding and the heat affected zone (HAZ) of SA508 cl.3 steel were investigated through the use of TEM, tensile and small punch (SP) tests. The specimens were irradiated at 563 K up to the neutron fluences of 5.79×10^{19} n/cm^2 (>1MeV). The microstructure of the clad was mainly composed of a fcc γ-phase, a low percentage of bcc δ-ferrite, and a brittle σ-phase. Along the weld fusion line there formed a heavy carbide precipitation with a width of 20~40 μm, showing preferential cracking during plastic deformation. The yield stress and ductile-to-brittle transition temperature (DBTT) of the irradiated clads increased. The origin of the hardening and the shift of the DBTT are discussed in terms of the irradiation-produced defect clusters of a fine size and brittle σ-phase.

KEYWORDS : RPV Cladding, Neutron Irradiation, 309L, SA508cl.3, HAZ

1. INTRODUCTION

Irradiation-induced embrittlement of the cladding and heat affected zone (HAZ) of a reactor pressure vessel (RPV) steel was investigated through the utilization of HANARO and JMTR. The inner wall of the nuclear RPV was cladded in 300 grade austenitic stainless steels with a thickness of a few millimeters in order to prevent a general corrosion attack on the ferritic low alloy steel as well as to prevent radioactive contamination problems in the main coolant systems. The presence of the cladding requires additional information regarding the material properties before the RPV safety can be assessed, and the properties of the cladding are considered to be influenced by the in-service exposure to high energy neutron irradiation at the reactor operating temperature [1,2]. In addition, the HAZ was produced in RPV steels as a result of stainless steel cladding, and showed relatively complex microstructures [3,4]. Therefore, understanding of the mechanical property changes in cladding and the HAZ of RPV steel under neutron irradiation is an important factor for a safe and extended service life of a reactor operation.

In this study, the microstructural characteristics and their effects on the mechanical property changes by neutron irradiation were characterized by transmission electron microscopy (TEM), tensile and small punch (SP) tests.

2. EXPERIMENTAL

2.1 Materials Fabrication

The materials used were a type ER309L stainless steel weld metal and low-alloyed SA 508 cl.3 RPV steel. The chemical compositions are listed in Table 1. Three kinds of RPV claddings were produced with submerged arc welding on SA508 cl.3 plates by varying the heat input

Table 1. Chemical Compositions of the ER309L Weld Metal and the SA508 cl.3 RPV Steel (wt. %)

	C	Si	Mn	P	S	Cr	Ni	Mo	Co	V	Ti	Cu	Nb	N	Fe
ER309L	0.011	0.36	1.60	0.013	0.001	23.77	13.19	0.06	0.026	0.052	0.09	0.039	<0.01	0.045	bal.
SA508 cl.3	0.17	0.10	1.35	0.006	0.002	0.16	0.82	0.50	-	0.004	-	0.03	-	0.006	bal

Table 2. Volumetric Phase Fractions of Each RPV Cladding Depending on the Maximum Heat Input

Index	Max. heat input (kJ/cm)	γ-phase	*FN(before PWHT)	*FN(after PWHT)	**σ-phase(vol. %)
K001	164.4		9.1	6.6	1.9
K002	188.5	~90	10.2	6.0	3.7
K002J	188.5		10.4	2.5	7.9

* FN; ferrite number measured by magnetic gage, which nearly equals the volumetric percentage.

** The fraction of the σ-phase was determined by an image analyzer after electrolytic etching in a solution of 50g NaOH + 100ml water.

from 164.4 (K001 clad) to 188.5 kJ/cm (K002J clad). The clad plates were then post-weld heat treated (PWHT) at 893 ~ 901 K for 41 hours. The microstructure of the cladding was examined using a scanning electron microscope (SEM) after electrolytic etching in a solution of 50g NaOH in 100ml water at 2 V for 5 s. The volumetric phase fraction of the σ-phase ranged from 1.9 (K001 clad) to 7.9 vol. % (K002J clad). The phase fractions of each cladding are shown in Table 2.

2.2. Tensile and SP Tests

In the HAZ of low-alloyed SA508cl.3 steel, small size tensile (gage length = 5 mm, $1.2^{w} \times 0.25^{t}$ mm) and disk type ($3\varphi \times 0.28^{t}$ mm) small punch (SP) specimens were sampled 0, 3, 6, 9 and 20 mm away from a weld fusion line. Disk and coupon ($10 \times 10 \times 0.5$ mm^3) type SP specimens were also sampled 2 mm away from the weld fusion line in the RPV clads. SP tests were performed at a cross-head speed of 0.2 and 0.4 mm/min for disk- and coupon-type specimens, respectively, at temperatures ranging from 77 to 293K. Steel balls of 1 and 2.4 mm in diameter, in which the hardness values were over HRC 60, were employed to apply a load to the disk- and coupon-type specimens, respectively. The specific SP energy was evaluated as the area under the load-deflection curve per unit thickness of a given specimen, J/mm. The SP ductile-to-brittle transition temperature (SP-DBTT) was defined as the temperature where the specific SP energy was the average of the maximum SP energy and lower shelf energy. SEM was used to observe the cracking appearance of the specimens.

2.3. Neutron Irradiation

Disk-type SP and small-sized tensile specimens were neutron irradiated in a Japan Materials Testing Reactor (JMTR) at 563 ± 1K up to the fluence of 1.02×10^{19} n/cm^2 (>1MeV). Coupon-type SP specimens were irradiated at an identical temperature up to the fluence of 5.79×10^{19} n/cm^2 (>1MeV) by utilizing the Hi-Flux Advanced Neutron Application Reactor (HANARO) in Korea.

3. RESULTS AND DISCUSSION

3.1. Microstructural Characteristics

Fig. 1 presents a typical microstructure of 309L cladding that varies with the heat input rate during submerged arc welding, indicating that the claddings were composed of nearly 90 % fcc austenite, a small percentage of bcc δ-ferrite, and a brittle σ phase. The δ-ferrite mainly formed at the austenite grain boundaries. As listed in Table 2, the higher heat input prior to PWHT (K002 and K002J sample) resulted in a slightly larger percentage of δ-ferrite compared to the lower sample (K001).

After the stress-relieving heat treatment, the content of δ-ferrite was reduced to approximately 6.6, 6.0 and 2.5 vol. % in the K001, K002 and the K002J clad, respectively, while the total amount of the σ phase was measured to be approximately 1.9, 3.7 and 7.9 vol. %, respectively (Table 2) for these samples. For the K002J cladding, the initial δ/γ boundaries moved into the δ-ferrite, and what remained was nearly all transformed to σ and new austenite (γ、)

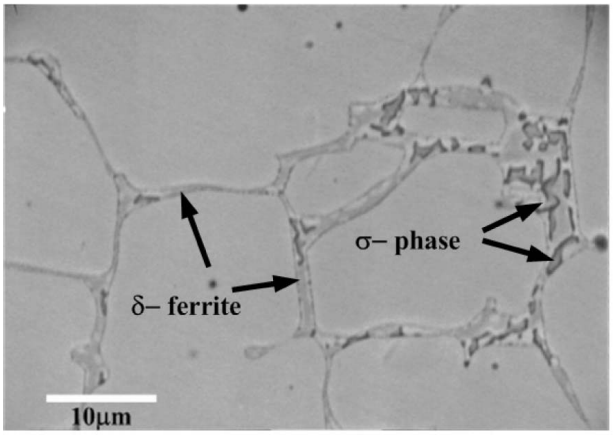

Fig. 1. Typical Microstructure of K001 RPV Clad. Gray is the γ-phase, Dark Gray is the δ-ferrite, and Black is the σ-phase

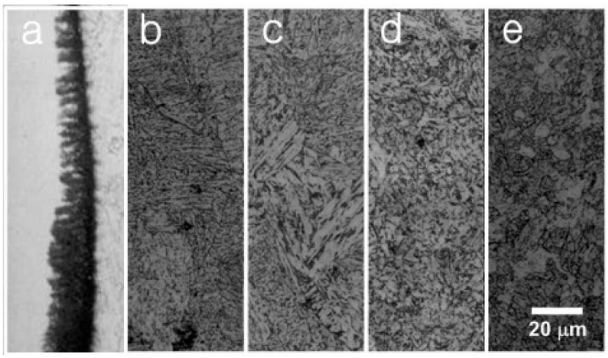

Fig. 2. Optical Microstructures of HAZ in SA508cl.3 RPV Steel, Sampled From (a) the Fusion Boundary (b) 0 mm (Coarse-grained), (c) 3 mm (Fine-grained), (d) 6 mm (Intercritical) and (e) 9 mm (Subcritical) Away From a Weld Fusion Line. Nital Etching(2% HNO_3+98% Ethanol)

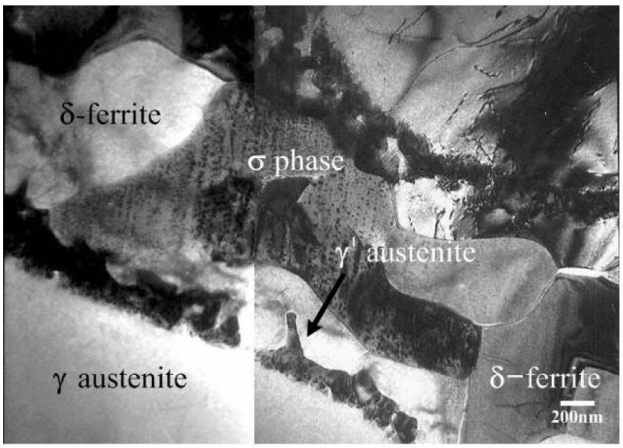

Fig. 3. Transmission Electron Micrographs of the K002 RPV Cladding; Fluence = 5.79×10^{19} n/cm^2 (>1MeV)

during PWHT. At the same time, the formation of σ in the K001 cladding was not significant.

The HAZ of SA508cl3 is "scallop-shaped", and the maximum width is approximately 10 mm. The HAZ was composed of a variety of microstructures with various grain and precipitate sizes [4]. Fig. 2 presents the optical microstructures as a function of the distance from the overlay weld fusion line. The base metal consists of a tempered bainite structure, and the ASTM grain size number and RT_{NDT} of the material are 7.0 and -30F, respectively. As the cladding is approached, the base metal experiences slight changes in the microstructure, which result from slight heating into the austenite region. Closer to the cladding, the material is heated further during cladding; thus, more of the ferrite is transformed into austenite. Finally, the entire structure is heated in the austenite region, transforming it into fine grains of ferrite and bainite as it cools. Close to the fusion line, the material is heated to a higher temperature, and forms coarse austenite grains that transform to an acicular bainitic structure upon cooling. In addition, along the weld fusion line, a heavy carbide precipitation zone with a width of 20~40 μm (Fig. 2a) formed.

Fig. 3 shows TEM micrographs of the δ-ferrite phase, γ-phase and σ-phase in the K002 clad. Although both the δ-ferrite and γ phases were hardened by neutron irradiation, visible defect clusters could not be observed in these phases, suggesting that the defect clusters contributing to the hardening by irradiation are too small to be observed by TEM, meaning that they are smaller than 1 nm. In contrast, many small dot- like structures were observed in the σ-phase. It proved difficult to identify the characteristics of these dot-like structures; however they are thought to possibly be small dislocation loops formed in the σ-phase.

3.2. Tensile Properties

Fig. 4 shows the dependence of tensile strength and ductility at room temperature on the neutron fluence. The K002J cladding showed a higher yield stress (σ_y) compared to the K001 sample in an unirradiated condition, with a difference of approximately 24 MPa. After irradiation, the σ_y value increased in both samples. The increment in yield stress ($\Delta\sigma_y$) was nearly 66 MPa at 5.1×10^{18} and 84 MPa at 1.02×10^{19} n/cm^2 (>1MeV) in the K001 cladding, while these values for K002J were approximately 45 and 40 MPa, respectively. The higher yield stress in the unirradiated K002J specimen was thought to have resulted from the larger fraction of the hard σ-phase (~ 7.9 %), and the irradiation hardening was due to the complex effect on both the δ-ferrite and γ austenite, although the cladding was composed of ~90 percent austenite phase.

The tensile strength (σ_{uts}) of K001 did not show any hardening effects after irradiation. This is due to irradiation-induced reduction in fracture stress that suppressed the work-hardening. For the K001 cladding, the σ_{uts} was nearly 500 MPa before and after irradiation, while the σ_{uts} for K002J was 522 MPa in an unirradiated condition. These values reduced to 487 and 457 MPa, respectively, according to the fluence.

As for the ductility change, neutron irradiation reduced the elongation. After irradiation, the plastic fracture strain (ε_f) in the K001 cladding was reduced to 76 and 67% compared to the unirradiated specimen. However, the ductility of K002J was much smaller than that of K001 even in an unirradiated condition. It measured nearly 56%, and was reduced to 43 and 42% by the irradiation. It is worth noting that the ductility of K002J in an unirradiated condition

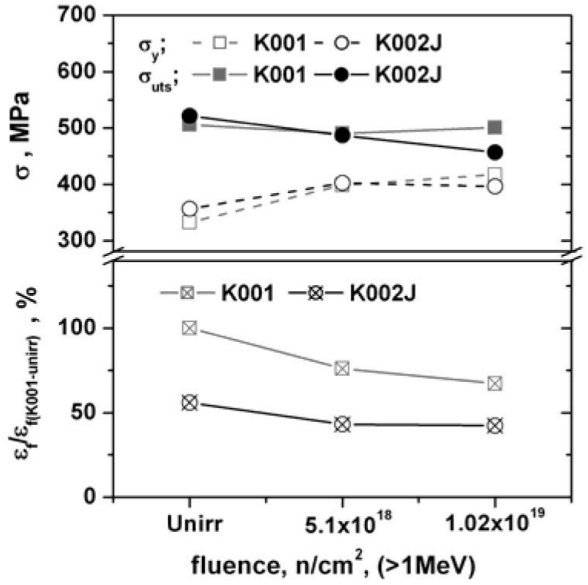

Fig. 4. Variations of Yield Stress (σ_y), Tensile Strength (σ_{uts}) and Fracture Strain (ε_f) as a Function of Neutron Fluence in RPV Cladding

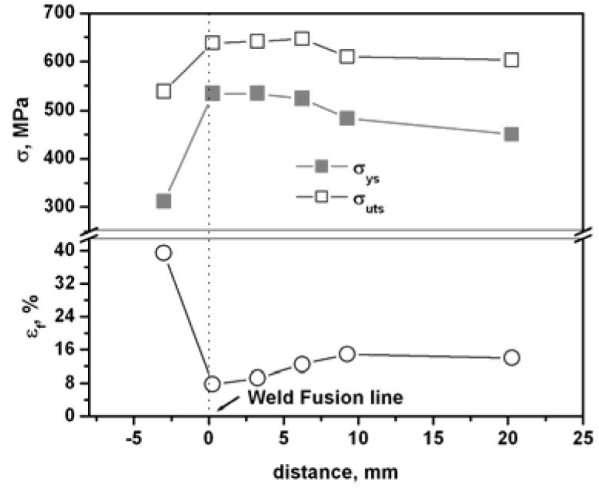

Fig. 5. Changes in Yield (σ_{ys}), Tensile Strength (σ_{uts}) and Fracture Strain (ε_{pf}) as a Function of the Distance From Weld Fusion Line in the RPV HAZ

remained lower than that of the irradiated K001 cladding.

Each HAZ shows different tensile properties, as each has completely different microstructures. Fig. 5 presents the yield (σ_{ys}), tensile strength (σ_{uts}) and plastic fracture strain (ε_{pf}) as a function of distance from the weld fusion line.

As the cladding is approached, the yield and tensile strength increased gradually from 450 to 530, and 600 to 640 MPa, respectively. At the same time, the plastic fracture strain reduced by approximately half, from 14 to 8 percent.

3.3. Ductile to Brittle Transition Behavior

The effects of the σ-phase and neutron irradiation on the SP energy of the claddings are shown in Fig. 6. The SP-DBTT was 144 and 165 K in the K001 and in K002 clad, respectively. The difference in SP-DBTT between the claddings is attributed to the different amount of σ-phase that will play a role in the crack initiation by fracturing at an early stage of deformation. After irradiation, the SP-DBTT moved to a higher temperature. However, as shown in Fig. 6, the increase in SP-DBTT (SP-ΔDBTT) is nearly saturated irrespective of the neutron fluence such that the SP-ΔDBTT is approximately 14 K. The cracking appearance of the SP specimens were changed from circumferential cracking to radial cracking as a function of the test temperature, content of the σ-phase and the neutron irradiation. As shown in Fig. 6, in the unirradiated K001 cladding, the cracking appearance was completely circumferential at room temperature, and it showed a mixed mode of circumferential and radial cracking below the transition temperature region. Similar results were also observed in the K002 specimens except that the dominant cracking was radial at 77 K.

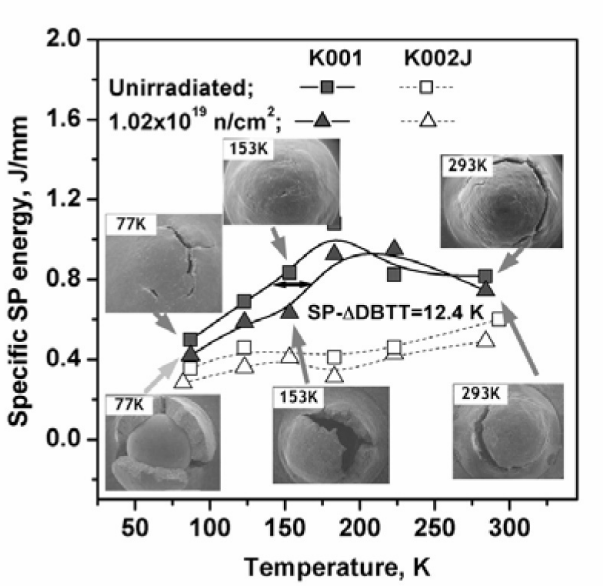

Fig. 6. Variations in the SP Energy and Cracking Appearance of the K001 Cladding. The Three Upper and Lower Photos Correspond to the States Before and After Irradiation, Respectively

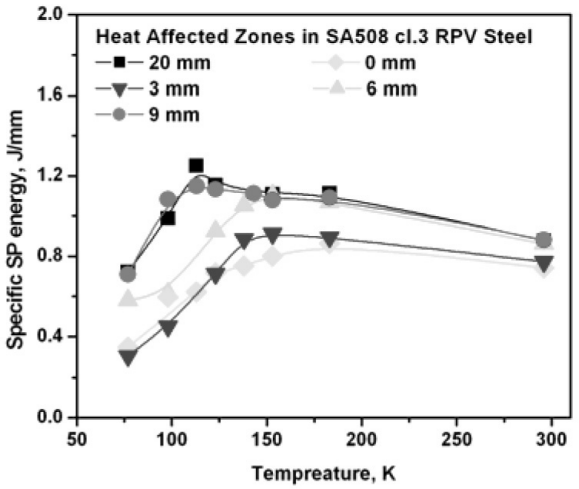

Fig. 7. Changes in Specific SP Energy in SA508cl.3 RPV Steel HAZ as a Function of Test Temperature

Conversely, the cracking appearance of the K002J specimens was completely radial except for those tested at room temperature. After irradiation, although the same transition behavior of cracking was observed in the K001 cladding, the radial cracking became much more dominant as the test temperature decreased. Complete radial cracking was observed at 77 K. The transition temperature where the cracking appearance changed from circumferential to radial also shifted to higher values in the K002 cladding, while complete radial cracking was shown in the K002J cladding at all test temperatures. These changes in the cracking appearances are related to the changes in the principal stress combined with the fracture stress of each phase. Detailed information can be found in a previous work by the authors [5].

The ductile-to-brittle transition behavior of each HAZ as a function of the test temperature is shown in Fig. 7. In the 9 (subcritical HAZ) and 20 mm (base metal) conditions, an identical transition behavior was observed, showing a gradual increase in SP energy in decreasing temperatures, to a maximum temperature at nearly 113 K. At that point, a sudden drop of SP energy was observed as the test temperature decreased further. However, a lower shelf SP energy could not be obtained until the test temperature reached 77 K. For the 6 mm (intercritical) HAZ, it also showed very similar SP energy, with 20 and 9 mm conditions until the test temperature reached 153 K. Moreover, the SP energy decreased with further cooling. The lowest SP energy in the HAZ regions was observed for the specimens sampled 0 and 3 mm away from the fusion line, corresponding to a coarse- and fine-grained HAZ, respectively. These revealed the lowest toughness for all test temperatures in addition to the highest ductile-to-brittle transition temperature compared to all other specimens. The embrittled nature appears to be associated with the change of grain size, number density and morphology of the carbides as well [6]. In addition, as shown in Fig. 8, the heavy carbide precipitation zone between the 309L cladding and the SA508 cl.3 steel revealed a significantly embrittled nature, as they cracked during plastic deformation in the SP tests.

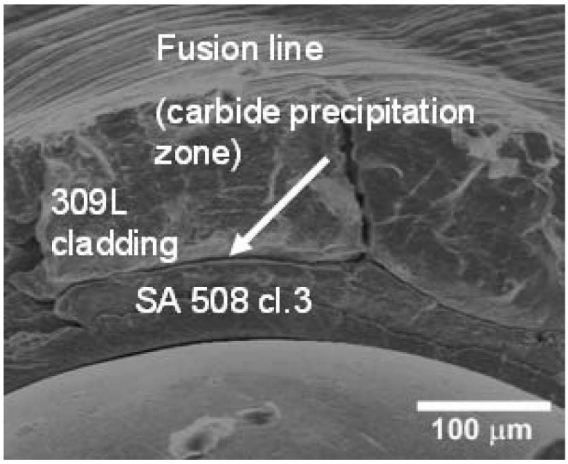

Fig. 8. Formation of Cracks Between 309L Cladding and SA508 cl.3 Steel, Tested at 153K

4. CONCLUSIONS

The experimental results of irradiation effects on the mechanical properties of cladding and HAZ of RPV steel were obtained as a function of the test temperature and neutron irradiation. The following main conclusions can be drawn.

- The microstructure of the 309L clad was composed mainly of fcc γ-phase, a small percentage of bcc δ-ferrite, and a brittle σ-phase. The HAZ in SA508cl.3 was composed of a variety of microstructures with various grain sizes and precipitates. In addition, along the weld fusion line, a heavy carbide precipitation zone with a width of 20~40 μm formed.
- After neutron irradiation on the cladding, the yield stress in addition to the SP ductile-to-brittle transition temperature (SP-DBTT) increased. However, the increase in SP-DBTT was nearly saturated, and was independent of the neutron fluence. Based on a TEM observation, the origin of the irradiation hardening was accounted for by the irradiation-produced invisible defect clusters of a very fine size (< 1~2 nm).
- As the specimen sampling position approached the weld fusion line in the HAZ of SA508 cl.3, an increase

in yield stress associated with a reduction in ductility was observed. In addition, significant cracking of the carbide precipitation zone was observed between the 309L cladding, and SA508.cl.3 was found during plastic deformation.

REFERENCES

[1] M.G. Hortsten, W.P.A. Belcher, Effect of Radiation on Materials: 20th International Symposium, ASTM STP 1405, S.T. Rosinski et. al. (Eds.), ASTM, West Conshohocken, 2001, p. 328.

[2] S. K. Iskander et al., Experimental Results of a Test to Investigate Flaw Behavior of Mechanically Loaded Stainless Steel Clad Plates, NUREG/CR-5785, April, 1992.

[3] F. M. Haggag, W.R. Corwin, R.K. Nanstard, Nucl. Eng. and Des. 124 (1990) 129-141.

[4] J.H. Kim, E.P. Yoon, Notch Position in the HAZ Specimen of Reactor Pressure Vessel Steel, Journal of Nuclear Materials 257 (1998) 303-308.

[5] I.S. Kim, J.S. Lee, A. Kimura, Embrittlement of ER309L Stainless Steel Cladding by σ-phase and Neutron Irradiation, Journal of Nuclear Materials 329-333 (2004) 607-611.

[6] J.S. Lee, I.S. Kim, S.C. Kwon, Evaluation of Microstructural and Mechanical Properties of SA508 cl.3 Heat Affected Zone Produced by RPV Cladding, Proceedings of Korean Nuclear Society Autumn Meeting, Yongpyung, Korea, October, 2004.